Time-Resolved in Situ Raman and Small-Angle X-ray Diffraction Experiments: From Silica-Precursor Hydrolysis to Development of Mesoscopic Order in SBA-3 Surfactant-Templated Silica†

Niki Baccile,[‡,⊗] Cilaine V. Teixeira,[§,#] Heinz Amenitsch,[||] Françoise Villain,[⊥] Mika Lindén,*[,§] and Florence Babonneau*[,‡]

Laboratoire de Chimie de la Matière Condensée de Paris (LCMCP), Université Pierre et Marie Curie-Paris 6 and CNRS, 4 place Jussieu, Paris, France, Department of Physical Chemistry, Åbo Akademi University, Turku, Finland, Institute of Biophysics and Nanosystems Research, Austrian Academy of Sciences, Graz, Austria, and Chimie Inorganique et Matériaux Moléculaires (CIM2), Université Pierre et Marie Curie-Paris 6 and CNRS, 4 place Jussieu, Paris, France

Received July 31, 2007. Revised Manuscript Received September 22, 2007

Time-resolved in situ Raman spectroscopy and small-angle X-ray diffraction have been combined in order to characterize the formation of hexagonal mesostructured SBA-3 silica. Experiments were performed under identical synthesis conditions in order to correlate the molecular and mesoscopic scales. Cetyltrimethylammonium bromide (CTAB) was used as the structuring agent with tetraethoxysilane (TEOS) as the silica precursor at a constant CTAB/TEOS molar ratio under highly acidic conditions and for various dilutions. Raman spectra allowed quantification of the release of ethanol that was produced solely by hydrolysis of TEOS under the experimental conditions used. The hydrolysis kinetics of TEOS was greatly enhanced in the presence of the surfactant as a result of micellar solubilization and surfactant stabilization of emulsion droplets. At the time of precipitation, the degree of TEOS hydrolysis depended strongly on the TEOS/CTAB concentration, decreasing with increasing concentration. The time evolution of the *d*-spacing and the full width at half-maximum of the (10) main reflection in the XRD pattern showed two distinct stages that were also strongly dependent on the sol composition. There seemed to be a coexistence of an ordered phase and a disordered one for a longer time in SBA-3 compared with MCM-41, clearly indicating that the ordering process is slower for SBA-3.

Introduction

Highly organized mesostructured silica-based materials are, at present, a widespread research topic. Since their discovery in the 1990s,[1,2] these materials have been studied primarily for their potential applications in preparing powders having very high specific surface areas with a range of chemical modifications on their exposed surfaces. The potential applications were initially thought to be primarily in catalysis, but then the range of applications was extended to include fields such as adsorption, sensing, encapsulation, and even electronics. More details on this topic are provided in several available high-quality reviews.[3,4]

Two major advantages that stimulated research in the field are the mild conditions employed and the ease of the steps involved in the synthesis of these materials. Nevertheless, the large number of publications on this topic has not yet entirely clarified all the details concerning their formation mechanisms, which involve several sequential and/or simultaneous events that occur on different length scales: the silica polycondensation process, interactions between amphiphilic moieties and inorganic species, development of micellar structure, formation of long-range order, and precipitation of the final product having a given shape and morphology.

Table 1 lists the characterization techniques heretofore reported in the literature to have been used for investigating the formation mechanisms of various silica/surfactant mesophases. The table also indicates the main structural output(s) associated with each method. The molecular level is best characterized by spectroscopic techniques such as electron paramagnetic resonance (EPR), NMR, IR, and fluorescence, while small-angle X-ray scattering/X-ray diffraction (SAXS/XRD) together with transmission electron microscopy (TEM) specifically targets the mesoscale.

The suitability of these methods for in situ time-resolved investigations has also been evaluated. Suitable methods should allow in situ study of the reactive medium without

† Part of the "Templated Materials Special Issue".

* Corresponding authors. E-mail: mlinden@abo.fi and fb@ccr.jussieu.fr.
‡ LCMCP, Université Pierre et Marie Curie-Paris 6 and CNRS.
§ Åbo Akademi University.
|| Austrian Academy of Sciences.
⊥ CIM2, Université Pierre et Marie Curie-Paris 6 and CNRS.
⊗ Present address: Max-Planck Institute for Colloids and Interfaces, Golm, Germany.
Present address: Unitat de Biofisica, Facultat de Medicina, Universitat Autonoma de Barcelona, Barcelona, Spain.

(1) Beck, J. S.; Vartuli, J. C.; Roth, W. J.; Leonowicz, M. E.; Kresge, C. T.; Schmitt, K. D.; Chu, C. T. W.; Olson, D. H.; Sheppard, E. W. *J. Am. Chem. Soc.* **1992**, *114*, 10834.
(2) Huo, Q.; Margolese, D. I.; Ciesla, U.; Feng, P.; Gier, T. E.; Sieger, P.; Leon, R.; Petroff, P. M.; Schueth, F.; Stucky, G. D. *Nature* **1994**, *368*, 317.
(3) Soler-Illia, G. J. d. A. A.; Sanchez, C.; Lebeau, B.; Patarin, J. *Chem. Rev.* **2002**, *102*, 4093.
(4) Patarin, J.; Lebeau, B.; Zana, R. *Curr. Opin. Colloid Interface Sci.* **2002**, *7*, 107.

10.1021/cm702128u CCC: $40.75
Published on Web 12/23/2007

Table 1. Evaluation of Experimental Techniques Described in the Literature for Performing Time-Resolved in Situ Studies on Mesostructured Silica Powders Obtained by Precipitation in Solution (the Number of + Signs Indicates the Suitability of the Technique for in Situ and/or Time-Resolved Studies)

		measurement suitability	
technique	output(s)	in situ[a]	time-resolved[b]
TEM	micelle aggregates; ordering	−	+ +
SAXS/XRD	shape of aggregates; ordering	+ + +	+ + +
EPR	organic/inorganic interactions; micelle aggregates	+ (+)	+ + +
DLS	apparent aggregate size	+ (+)	+
Fluorescence	organic/inorganic interactions; micelle aggregates	+	+ + +
NMR			
^{1}H	surfactant mobility	+ +	+ +
^{2}H	ordering; mesophase	+	+ +
^{29}Si	extent of hydrolysis/ condensation	+ +	−
^{17}O	hydrolysis	−	+ +
^{14}N	mesophase growth	+	+
FT-IR	reactivity of inorganic species	+	+ + +
Raman	reactivity of inorganic species	+ + +	+ + +

[a] Each + sign corresponds to one of the following characteristics: (1) no modification of chemical composition (e.g., dilution, use of D_2O, use of TMOS instead of TEOS, etc.) is required; (2) no external species (e.g., paramagnetic or fluorescence probes, etc.) are introduced into the reacting medium; (3) no modification of the synthesis process (e.g., no stirring, smaller reaction volumes, etc.) is needed. [b] Each entry indicates the characteristic measurement time (t_m) of the related technique according to the following key: + + +, $0 < t_m < 10$ s; + +, 10 s $< t_m < 1$ min; +, 1 min $< t_m < 10$ min; −, $t_m > 10$ min.

any modification of its chemical composition and processing parameters. This is the key to ensuring good reliability of the proposed formation mechanism. We estimate that the system should be adapted as seldom as possible to the technique, as discussed in more detail in the next paragraph. The suitability of the methods as in situ techniques was thus evaluated according to three criteria: (1) the need to change the chemical composition of the starting system; (2) the need to introduce external species required for the technique to be effective; and (3) the need to modify processing parameters, such as the type of reaction container, the stirring speed, and so on. Suitable investigative methods should also require measurement times compatible with the kinetics of the events that one would like to follow. Real-time tracking of the evolving system is preferable to periodic snapshots or to a response that has been averaged over a period of time during which the system undergoes many changes. The suitability of the methods for time-resolved studies was thus estimated from their characteristic measurement times. It is obvious that time-resolved experiments on systems that react rapidly will be more delicate than those for systems that evolve slowly.

To complete Table 1, in the following paragraphs we provide for each technique additional specific comments that have been suggested by analysis of the experimental conditions in some of the most relevant in situ studies that have been published.

TEM. Transmission electron microscopy offers a convenient way to observe micelles, particularly the evolution of their shapes with time as well as their long-range organization to form mesostructures at different moments during their synthesis.[5] However, specimen preparation is a key issue in order to ensure observations representative of the solution structures. For this reason, cryo-TEM, a powerful tool for investigating nanostructures in soft materials, has also been used to study silica/surfactant hybrid systems.[6,7] A negative point regarding TEM concerns the fact that this method is not a truly in situ approach, since it only provides snapshots at chosen reaction times. Nevertheless, snapshots can furnish quite a good representation of the reaction status at a given moment, provided that a quenching step is included in the synthesis procedure.

SAXS/XRD. Small-angle X-ray scattering/X-ray diffraction is clearly the best technique for studying micellar structures and shapes having short- and long-range order. Short acquisition times and an adaptable experimental setup have made it the most-used technique in time-resolved[8,9] and even temperature-resolved[10,11] in situ experiments. Nevertheless, the acquisition times required when using low-flux X-ray sources are not compatible with the requirements for time-resolved measurements, as shown in 1998 by Lindén et al.[12] Hence, SAXS/XRD experiments must be performed using a high-flux X-ray source such as synchrotron radiation, making this type of experiment quite expensive and difficult to access. Energy-dispersion X-ray diffraction was used on SBA-1 materials,[13] but poor resolution hindered the evaluation of detailed mesophase parameters.

EPR Spectroscopy. Electron paramagnetic resonance spectroscopy has been used to obtain information about silica/micelle interactions during material formation. This technique, used extensively by the Goldfarb[14,15] and Ottaviani[16] groups, can be considered truly time-resolved as a result of its very high sensitivity for even a small amount of a paramagnetic species. As far as its suitability as an in situ approach is concerned, introduction of an external probe with a paramagnetic center provides an extra parameter that must be taken into account. In addition, experimental synthesis conditions must be adapted to meet EPR apparatus requirements: use of either flat cells or tubes results in smaller reaction volumes where no stirring is available, making this setup unsuitable for a number of established experiments.

(5) Díaz, I.; Alfredsson, V.; Sakamoto, Y. *Curr. Opin. Colloid Interface Sci.* **2006**, *11*, 30.
(6) Regev, O. *Langmuir* **1996**, *12*, 4940.
(7) Ruthstein, S.; Schmidt, J.; Kesselman, E.; Talmon, Y.; Goldfarb, D. *J. Am. Chem. Soc.* **2006**, *128*, 3366.
(8) Ågren, P.; Lindén, M.; Rosenholm, J. B.; Schwarzenbacher, R.; Kriechbaum, M.; Amenitsch, H.; Laggner, P.; Blanchard, J.; Schüth, F. *J. Phys. Chem. B* **1999**, *103*, 5943.
(9) Flodström, K.; Teixeira, V. T.; Amenitsch, H.; Alfredsson, V.; Lindén, M. *Langmuir* **2004**, *20*, 4885.
(10) Gross, A. F.; Ruiz, E. J.; Tolbert, S. H. *J. Phys. Chem. B* **2000**, *104*, 5448.
(11) Tolbert, S. H.; Landry, C. C.; Stucky, G. D.; Chmelka, B. F.; Norby, P.; Hanson, J. C.; Monnier, A. *Chem. Mater.* **2001**, *13*, 2247.
(12) Lindén, M.; Schunk, S. A.; Schüth, F. *Angew. Chem., Int. Ed.* **1998**, *37*, 821.
(13) Egger, C. C.; Anderson, M. W.; Tiddy, G. J. T.; Casci, J. L. *Phys. Chem. Chem. Phys.* **2005**, *7*, 1845.
(14) Zhang, J.; Luz, Z.; Goldfarb, D. *J. Phys. Chem. B* **1997**, *101*, 7087.
(15) Ruthstein, S.; Frydman, V.; Kababya, S.; Landau, M.; Goldfarb, D. *J. Phys. Chem. B* **2003**, *107*, 1739.
(16) Galarneau, A.; di Renzo, F.; Fajula, F.; Mollo, L.; Fubini, B.; Ottaviani, M. F. *J. Colloid Interface Sci.* **1998**, *201*, 105.

Dynamic Light Scattering. Dynamic light scattering (DLS) has occasionally been used to follow the evolution of overall micelle size during the self-assembly process, according to evidence provided in ref 17 and references therein. The time scale of DLS measurements must fall in the minute range in order to obtain exploitable significant results. DLS has been adapted to the in situ approach, but caution must be taken in its use since DLS experiments take place in a smaller volume without stirring. In addition, the solutions generally need dilution in order to increase reaction times and prevent powder precipitation in the very first minutes of the reaction.

Fluorescence Spectroscopy. Fluorescence spectroscopy has been used to observe ion-exchange mechanisms at the micelle−silica palisade in order to better understand organic/inorganic interactions.[18] Even if the time scale for signal detection is very short, this technique has some drawbacks as far as in situ analysis is concerned: a well-chosen fluorescent probe must be introduced in the system, the solution must be kept transparent at all times, and the solution must be placed in a sample holder. The experiments proposed in ref 18 were performed using pH conditions under which no precipitation took place.

NMR Spectroscopy. Nuclear magnetic resonance spectroscopy has been used to study the liquid state in order to reach a wide range of objectives that depend on the nucleus under study. Unfortunately, this technique suffers from several general drawbacks: (1) Confined volumes in NMR tubes do not permit stirring of the solution. (2) Precipitation should be avoided, which requires working with systems that either react slowly (e.g., Pluronic-structured materials) or have been modified (e.g., by changing the pH or by dilution). (3) The low sensitivity for some nuclei requires isotopic enrichment, which increases the overall cost and introduces external species and/or synthetic steps. (4) Long relaxation times increase measurement times. Despite these difficulties, NMR studies have provided interesting results on various silica/surfactant systems:

^{1}H Studies. ^{1}H NMR spectroscopy was exploited by Flodström et al.[19] to follow the decrease in line width of the signal from the methyl group of the propylene oxide (PO) part of the Pluronic P123 surfactant during the synthesis of a hexagonal *p6mm* silica/Pluronic mesophase. They attribute this behavior to a decrease in mobility of the PO methyl group resulting from either the formation of large aggregates or interactions between the Pluronic surfactant and growing silica. The study of protons gives quite reasonably short acquisition times, making the time-resolved approach feasible.

^{2}H and ^{14}N Studies. Quadrupolar nuclei such as ^{2}H and ^{14}N can be used to identify the surfactant mesophase geometry in the presence of silicate species by examination of quadrupole interaction parameters. Firouzi et al.[20] used ^{2}H-enriched quaternary ammonium salts, while Egger et al.[13] studied the ^{14}N signal from the polar head groups of the cationic surfactant. The only drawback to the use of ^{2}H is the necessity of isotopic labeling of the sample.

^{29}Si Studies. ^{29}Si can be used to follow hydrolysis and condensation of the silica precursors and formation of the silica network in solution. This approach, which was tested in refs 13 and 20, for example, is far from being time-resolved, as a result of the low abundance, low sensibility, and long relaxation time of the ^{29}Si nucleus.

^{17}O Studies. ^{17}O was also used by Egger et al.[13] to follow water reactivity and oxygen localization in silica structured using quaternary ammonium salts. Here, the difficulties are the costs of the necessary ^{17}O isotopic enrichment and the drastic decrease in the water content of the starting solution required to minimize these costs.

FT-IR Spectroscopy. Fourier-transform infrared (FT-IR) spectroscopy could be a perfect technique for time-resolved in situ experiments because of its fast response. Unfortunately, the strong absorptions of far- and mid-IR radiation by water make necessary the use of sensitive attenuated total reflection (ATR) sampling devices, which are not compatible with true in situ measurements. Nevertheless, the ATR−FTIR method was effective in providing qualitative data regarding the species present during hydrolysis and condensation of TEOS under water-rich conditions.[21] The solvent spectra were subtracted from the sample spectra in order to better visualize the absorption bands for the species of interest. The ATR−FTIR technique was also used to follow the synthesis of mesoporous silica in fatty acid/aminoalkoxysilane/water systems.[22] However, strong overlap of bands from multiple species present in the solution made any quantitative analysis quite unreliable in that work.

Raman Spectroscopy. Raman spectroscopy can be used to follow hydrolysis of inorganic precursors as a function of time. Time-resolved data acquisition is possible because of the fast response of the Raman signal,[23] and new Raman spectrometers can be perfectly adapted to the setup required for these experiments. The main positive feature of this method is the fact that it does not detect the H−O−H angular-deformation vibration band of water,[24] but in all cases, nonfluorescing and limpid solutions are required. Raman spectroscopy has not yet been adapted for use in time-resolved in situ studies of mesostructured silica materials.

Most of the in situ mechanistic studies performed to date have concentrated on a single type of observation, and correlations between them are difficult to establish because of the differences in experimental conditions and chemical compositions of the systems studied. As we will discuss in a later section, one important experimental parameter is the solution stirring rate, which plays a key role in the kinetics of the self-assembly process. None of the techniques listed above allow stirring, except for SAXS/XRD and Raman

(17) Mesa, M.; Sierra, L.; Guth, J.-L. *Microporous Mesoporous Mater.* **2007**, *102*, 70.
(18) Frasch, J.; Lebeau, B.; Soulard, M.; Patarin, J.; Zana, R. *Langmuir* **2000**, *16*, 9049.
(19) Flodström, K.; Wennerström, H.; Alfredsson, V. *Langmuir* **2004**, *20*, 680.
(20) Firouzi, A.; Atef, F.; Oertli, A. G.; Stucky, G. D.; Chmelka, B. F. *J. Am. Chem. Soc.* **1997**, *119*, 3596.
(21) Tejedor-Tejedor, M. I.; Paredes, L.; Anderson, M. A. *Chem. Mater.* **1998**, *10*, 3410.
(22) Rodriguez-Abreu, C.; Izawa, T.; Aramaki, K.; Lopez-Quintela, A.; Sakamoto, K.; Kunieda, H. *J. Phys. Chem. B* **2004**, *108*, 20083.
(23) Marino, I.-G.; Lottici, P. P.; Bersani, D.; Raschella, R.; Lorenzi, A.; Montenero, A. *J. Non-Cryst. Solids* **2005**, *351*, 495.
(24) Rull, F. *Pure Appl. Chem.* **2002**, *74*, 1859.

spectroscopy. However, in order to obtain a better overview of the formation process at various length scales, efforts have recently been made to combine complementary techniques: NMR with TEM[19] and also with XRD,[13] IR with SAXS/XRD,[22] and EPR with cryo-TEM.[7] As the Goldfarb group has already pointed out,[7] in such studies it is important to carry out the experiments under the same reaction conditions in order to allow correlation between the two length scales. It is also essential to avoid any major modifications of the synthetic conditions used to prepare the mesoporous materials. Indeed, most of the studies combining various techniques have been performed on systems that react slowly, for which measurement times on the order of minutes are compatible with the observed reaction kinetics. This is typically the case for the formation of SBA-15.[9,25] For systems that react rapidly, such as those involving cationic surfactants for which precipitation occurs within a few minutes, the choice of time-resolved in situ techniques is somewhat limited.

Following the pioneering work of the researchers from Mobil,[1] several mechanisms related to the synthesis of mesostructured silica-based materials under alkaline conditions have been proposed. The first proposal was based on the supposed existence of a preformed liquid crystalline phase, but this idea was shown to be wrong by Chen et al.,[26] who used ^{14}N NMR spectroscopy to prove that no hexagonal mesophase pre-exists in solution before addition of the silica source. The second proposal assumed a cooperation mechanism between silicates and hexagonal micelles that had preformed in the solution, which eventually contributed to building up the hexagonal mesostructure with long-range order. Next, the charge-density-matching mechanism was proposed by the Stucky and Chmelka groups.[27,29] They explained that electrostatic interactions first occur between surfactant polar heads and multiply charged silicate oligomers in solution. Because of high surface-charge density, the organic/inorganic mesophase formed from the condensing silica species must pass through a low-curvature lamellar phase before reaching the higher-curvature 2D-hexagonal phase. This picture was similar to the previous observation in 1990 by Yanagisawa et al.[29] of a progressive phase transformation from lamellar to hexagonal in kanemite upon addition of ammonium ion salts containing long alkyl chains. Later in the 1990s, several interesting studies carried out using in situ techniques after preventing the silicate species from undergoing extensive condensation reported a self-assembling phenomenon between silicates and surfactant micelles. Firouzi et al.[28] used NMR and neutron-scattering techniques to demonstrate the formation of cylindrical micelles from spherical ones upon addition of silicate to the starting solution. Galarneau et al.[16] used EPR spectroscopy in the presence of well-chosen paramagnetic probes to prove that an exchange between silicate anions and surfactant counterions occurs at the micelle double-layer interface, while Frasch et al.[18] used fluorescence techniques to show that ion exchange is quite limited at the micelle double-layer interface but enhanced when the surfactant molecule is alone in solution. Micelles only play the role of surfactant reservoirs and do not serve as "building blocks" of the whole structure. It is important to repeat that these studies investigated only MCM-41-type materials, in which direct electrostatic interaction occurs between negatively charged silica and positively charged ammonium surfactants.

On the contrary, the literature regarding synthesis of mesostructured silica-based materials under acidic conditions is not as abundant. This type of synthesis was proposed by Huo et al.[2] and leads to the formation of the SBA-1 (cubic *Pm*3*n*), SBA-2 (3D-hexagonal $P6_3/mmc$), and SBA-3 (2D-hexagonal, *P*6*m*) surfactant/silica mesophases. In this case, interactions between silica and surfactant are of a different nature, since a negative counterion (coming from the surfactant or from the acid used) interposes between the positively charged micelles and the quasi-neutral silica surface.[30] Important work in this area was performed by Egger et al.,[13] who investigated the formation mechanism of the cubic *Pm*3*n* SBA-1 phase obtained from TEOS and CTEAB (cetyltriethylammonium bromide). They combined in situ energy-dispersive XRD with multinuclear (^{29}Si, ^{17}O, ^{14}N) NMR techniques; however, they had to adapt the reactant molar ratios to these techniques in order to optimize the experiments, and the resulting ratios ended up being quite far from those for the SBA-1 synthetic conditions. Lesaint et al.[31] investigated the formation of the 2D-hexagonal SBA-3 mesophase using DLS. However, as already mentioned for this technique, they had to dilute the system to a much greater extent ($H_2O/Si = 734$) than was used in the original preparation from Huo et al.[2] ($H_2O/Si = 130$), and the acid concentration was consequently lower (0.5–0.9 M instead of 3.9 M). To date, no time-resolved in situ studies combining techniques that probe molecular as well as mesoscopic scales have been performed. We thus decided to reinvestigate the formation of SBA-3 in the same range of experimental conditions used by Huo et al.,[2] employing cetyltrimethylammonium bromide (CTAB) as the template and tetraethoxysilane (TEOS) as the silica precusor under highly acidic conditions. In view of Table 1, Raman spectroscopy and synchrotron SAXS/XRD seemed suitable complementary techniques for such rapidly reacting systems, since precipitation occurs within a few minutes. Time-resolved in situ SAXS/XRD using synchrotron radiation has already demonstrated its unique ability to track the appearance and development of long-range order in various silica/surfactant systems. Up to now, the weak point of the published studies has been the lack of information regarding the hydrolysis and condensation of the silica precursor. ^{29}Si NMR spectroscopy would be the optimum technique to

(25) Khodakov, A. K.; Zholobenko, V. L.; Impéror-Clerc, M.; Durand, D. *J. Phys. Chem. B* **2005**, *109*, 22780.
(26) Chen, C.-Y.; Burkett, S. L.; Li, H.-X.; Davis, M. E. *Microporous Mater.* **1993**, *2*, 27.
(27) Monnier, A.; Schüth, F.; Huo, Q.; Kumar, D.; Margolese, D.; Maxwell, R. S.; Stucky, G. D.; Krishnamurty, M.; Petroff, P.; Firouzi, A.; Janicke, M.; Chmelka, B. F. *Science* **1993**, *261*, 1299.
(28) Firouzi, A.; Kumar, D.; Bull, L. M.; Besier, T.; Sieger, P.; Huo, Q.; Walker, S. A.; Zasadzwinski, J. A.; Gluka, C.; Nicol, J.; Margolese, D. I.; Stucky, G. D.; Chmelka, B. F. *Science* **1995**, *267*, 1138.
(29) Yanagisawa, T.; Shimizu, T.; Kuroda, K.; Kato, C. *Bull. Chem. Soc. Jpn.* **1990**, *63*, 988.
(30) Baccile, N.; Laurent, G.; Bonhomme, C.; Innocenzi, P.; Babonneau, F. *Chem. Mater.* **2007**, *19*, 1343.
(31) Lesaint, C.; Lebeau, B.; Marichal, C.; Patarin, J.; Zana, R. *Langmuir* **2005**, *21*, 8923.

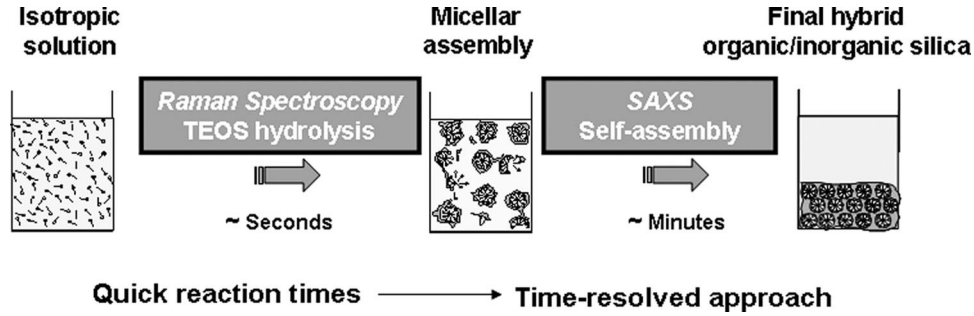

Figure 1. Schematic representation of the time-resolved in situ approach used in this work to study the formation of surfactant-templated silica powder.

Table 2. Systems Investigated in This Work

	reactant amounts (mol)				concentrations (M)		
system	TEOS	CTAB	HCl	H_2O	C_{Si}	C_{HCl}	C_{CTAB}
A	1	0.12	9.2	130	0.43	3.9	0.050
B	1	0.12	9.2	200	0.28	2.5	0.033
C	1	0.12	49.5	700	0.08	3.9	0.009

identify hydrolyzed and condensed species,[32] but its response time is not compatible with time-resolved study of the system of interest here. However, Raman spectroscopy is appropriate to follow the hydrolysis of a rapidly reacting silica precursor such as TEOS, even if previously reported Raman studies[23] were performed in the absence of templating agents, and thus on homogeneous solutions. This technique is thus appropriate prior to precipitation but unfortunately no longer continues to be effective once precipitated powder has formed. In the present work, combination of Raman spectroscopy and SAXS/XRD experiments allowed us to follow the various synthetic steps of the material synthesis, starting from time $t = 0$ (when the inorganic precursor was added to the surfactant solution) and continuing until the recovery of the precipitated silica/surfactant mesophase powder from solution (Figure 1). It is important to note that both techniques allowed us to observe the evolution of the system under stirring, so we were able to use them under the exact same synthetic conditions.

Experimental Section

Synthesis of Silica-Based Materials. All samples were prepared under acidic conditions using tetraethyl orthosilicate (TEOS, Aldrich) as the silica source and commercial CTAB (Aldrich) as the structuring agent. Molar ratios among all reactants were adapted from the original synthesis procedure of Huo et al.,[2] though several dilution conditions were tested, as indicated in Table 2. The synthesis procedure is detailed elsewhere.[30]

Characterization. Raman spectra were recorded using a Hololab 5000 R apparatus (Kaiser Optical Systems, Inc.) equipped with a 750 nm laser (power: 400 mW) connected to an optical fiber and also with a CCD camera. The Raman emission was collected at 180° with respect to the laser source. An optical lens system was used to focus the light at the center of the reaction beaker containing the aqueous solution of CTAB. The solution was continuously stirred, and the experiment was performed at room temperature. The time interval between data points was set to 5 s, and the start of the experiment (i.e., $t = 0$) occurred when TEOS was added to the solution. Data were acquired and treated with the HoloGRAMS software package. Small-angle X-ray diffraction experiments were conducted at the Austrian SAXS beamline of the ELETTRA synchrotron laboratory in Trieste, Italy.[33] The X-ray energy was 8 keV (1.54 Å), and the sample–detector distance was set to 955 mm. A CCD camera (X-ray Imager, Photonic Sciences, Oxford, U.K.) served as the detector, and silver behenate ($d = 58.37$ Å) was used for calibration. The framing rate was 10 s/frame, with typical exposure times of 4 s for all experiments. The reaction solution was circulated in a 1 mm quartz capillary using a batch-reactor/flow-through technique.[8] Because of the fast (3−5 min) mesostructuring process, data acquisition was stopped after 25 min of stirring, except in cases when powder aggregates formed earlier and stirring was stopped to prevent clogging of the 1 mm quartz capillary. All 2D images were corrected for detector artifacts (flat field, spatial corrections) and were integrated azimuthally using the FIT2D program.[34,35] The resulting 1D images were normalized for intensity fluctuations, and the instrument background was subtracted.

Results and Discussion

TEOS Hydrolysis Kinetics. Time-resolved in situ Raman spectroscopy was used to follow the hydrolysis kinetics of TEOS in highly acidic ($C_{HCl} \geq 2.5$ M) aqueous solutions of CTAB for three different compositions (Table 2).

The Raman spectra measured for CTAB/H_2O/HCl and CTAB/EtOH/H_2O/HCl solutions in which $C_{HCl} = 2.5$ M and $C_{CTAB} = 0.033$ M are shown in Figure 2. These concentrations were chosen to correspond to the solvent composition of system B, assuming complete TEOS hydrolysis (CTAB/EtOH = 0.12/4) for the second solution. The corresponding vibrational-mode assignments of the Raman Stokes bands are given in Table 3.[36–40] In the absence of ethanol (EtOH), the two most intense Raman bands of CTAB, located at 763 and 1063 cm^{-1} and assigned to the $N-CH_3$ rocking mode of the $N^+(CH_3)_3$ moiety and the C−C stretching mode, respectively, can hardly be detected because of the low CTAB concentration.[39] In the presence of EtOH (CTAB/EtOH = 0.12/4), three very strong peaks appear, located at

(32) Artaki, I.; Bradley, M.; Zerda, T. W.; Jonas, J. *J. Phys. Chem.* **1985**, *89*, 4399.
(33) Amenitsch, H.; Rappolt, M.; Kriechbaum, M.; Mio, H.; Laggner, P.; Bernstorff, S. *J. Synchrotron Radiat.* **1998**, *5*, 506.
(34) Hammersley, A. P.; Svensson, S. O.; Thompson, A.; Graafsma, H.; Kvick, Å.; Moy, J. P. *Rev. Sci. Instrum.* **1995**, *66*, 2729.
(35) Hammersley, A. P.; Svensson, S. O.; Hanfland, M.; Fitch, A. M.; Häusermann, D. *High Pressure Res.* **1996**, *14*, 235.
(36) Gnado, J.; Dhamelincourt, P.; Pélégris, C.; Traisnel, M.; Le Maguer Mayot, A. *J. Non-Cryst. Solids* **1996**, *208*, 247.
(37) Lippert, J. L.; Melpolder, S. B.; Kelts, L. M. *J. Non-Cryst. Solids* **1988**, *104*, 139.
(38) Matos, M. C.; Ilharco, L. M.; Almeida, R. M. *J. Non-Cryst. Solids* **1992**, *147−148*, 232.
(39) Kalyanasundaram, K.; Thomas, J. K. *J. Phys. Chem.* **1976**, *80*, 1462.
(40) Aarnoutse, P. J.; Westerhuis, J. A. *Anal. Chem.* **2005**, *77*, 1228.

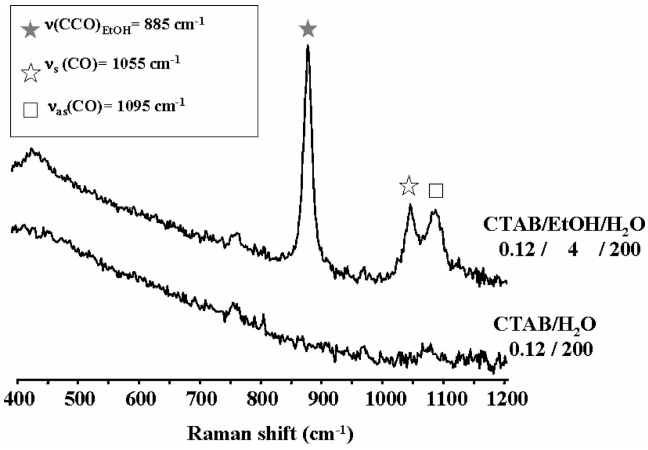

Figure 2. Raman spectra of CTAB solutions (C_{HCl} = 2.5 M): lower trace, CTAB/H_2O = 0.12/200; upper trace, CTAB/EtOH/H_2O = 0.12/4/200.

Table 3. Raman Bands of CTAB, EtOH, TEOS, and Silica Gel Reported in the Literature

species	wavenumber (cm^{-1})	assignment
CTAB[a]	763	CH_3 rock from $N^+(CH_3)_3$
	1063	C−C sym. stretch + CH_2 wag
EtOH[b]	436	C−C−O def.
	882	C−C−O stretch
	1050	C−O sym. stretch
	1090	C−O asym. stretch
TEOS[c]	656	SiO_4 sym. stretch
	800	SiO_4 asym. stretch
	933	C−C sym. stretch
	1094	C−O asym. stretch
TEOS-derived oligomers[b]	600	SiO_4 sym. stretch in $Si_2O(OEt)_6$
	576	SiO_4 sym. stretch in $Si_3O_2(OEt)_8$
	~545	SiO_4 sym. stretch in $Si_4O_3(OEt)_{10}$
silica gel[b]	~600	$Si(OSi)(OR)_3$ (R = H, Et)
	~540	$Si(OSi)_2(OR)_2$ (R = H, Et)
	~495	$Si(OSi)_3(OR)$ (R = H, Et)
	430	$Si(OSi)_4$

[a] Reference 39. [b] Reference 41. [c] Reference 38.

885, 1055, and 1095 cm^{-1} and assigned to the C−C−O stretch [ν(CCO)], C−O symmetric stretch [ν_s(CO)], and C−O asymmetric stretch [ν_{as}(CO)] modes of EtOH, respectively.[38] On the basis of these results, in subsequent analyses we were able to neglect the contribution made by the CTAB bands, and this feature, which depended strictly on our synthesis protocol, made the whole Raman spectrum clearer and much more legible.

Time-resolved Raman spectra were first recorded for a solution containing TEOS in the absence of CTAB (Figure 3a). The composition corresponded to that of system B (Table 2). An emulsion with rather large droplets remained throughout the experiment. The stirring speed (which was 300 rpm here) is thus a very important parameter influencing the reaction kinetics in these systems. Two main bands, located at 658 and 1095 cm^{-1} and assigned to TEOS[38] (Table 3), were observed. The spectral evolution with time shows the rapid decrease in the intensity of the band at 658 cm^{-1} and the appearance of two new bands located at 885 and 1055 cm^{-1}, which are characteristic of the release of EtOH molecules produced by hydrolysis of TEOS.

The time-resolved integrated intensities of the TEOS band at 658 cm^{-1} and the EtOH band at 885 cm^{-1} are shown in Figure 3b. The amount of EtOH released during the reaction was quantified. The intensity of measured Raman scattering of a substance A at irradiation frequency ν [$I(\nu)_{RA}$] can be analyzed according to eq 1:[40]

$$I(\nu)_{RA} = K(\nu)_A V C_A P_L \quad (1)$$

where C_A is the concentration of A in solution, V is the volume of the sample irradiated by the light source, P_L is the power density of the laser, and $K(\nu)_A$ is the absorption constant of substance A at irradiation frequency ν. This linear relationship is valid when no other object scatters light and when the sample does not absorb or emit at the irradiation frequency. We considered these conditions to be satisfied since the solution stayed clear during the whole process (i.e., for all $t \leq 300$ s) and neither gelation nor precipitation took place. In addition, none of the species present in the solution (water, TEOS, and EtOH) absorb or emit light at the irradiation frequency used here (the frequency corresponding to $\lambda = 750$ nm). Though we were unable to attribute absolute values to V and P_L, we hypothesized that these parameters kept the same values from one solution to another because the experimental setup remained unchanged. Given this hypothesis, only the product $X = K(\nu)_A V P_L$ needed to be determined in order to calculate C_A from the measured intensity $I(\nu)_{RA}$. In this work, the measured intensity was related to the EtOH concentration in water by means of a calibration curve, from which the experimental value $X_{EtOH} = 6678 \pm 440$ was found. We were able to use this value to calculate the experimental value C_{EtOH}^{exp} at any reaction time. For example, at $t = 300$ s, $C_{EtOH}^{exp} = 0.96 \pm 0.06$ M. If full hydrolysis is assumed, 4 EtOH molecules are produced per TEOS, which corresponds to the theoretical value $C_{EtOH}^{th} = 1.10$ M. Consequently at $t = 300$ s, 90% of the TEOS was hydrolyzed under the employed experimental conditions in the absence of surfactant. Theoretical Raman intensities corresponding to the release of 2, 3, or 4 EtOH molecules per TEOS are reported in Figure 3b. Interestingly, the TEOS band vanished after a reaction time of 120 s when slightly more than 3 EtOH molecules per TEOS were produced. Indeed, the band at 658 cm^{-1} only accounts for the symmetrical breathing mode of an SiO_4 tetrahedron [$\nu_s(SiO_4)$], which means that whenever a single Si−OEt bond is hydrolyzed, this signal can no longer be detected even if unhydrolyzed Si−OEt bonds are still present.[41] One would expect that when the overall TEOS signal is lost, the maximum EtOH concentration in solution would correspond to 1 EtOH molecule per silicon atom if one and only one Si−OEt bond per TEOS is hydrolyzed. In reality, TEOS coexists with species that have been submitted to multiple hydrolysis. This could be surprising, since it has been reported that in an excess of water, the concentration of Si−OEt groups rapidly tends to zero.[42] Moreover, the hydrolysis rate depends strongly on the degree of substitution of the monomers, with TEOS being the most reactive. But one should not forget that an emulsion remained throughout the reactions, which may indicate that TEOS molecules located in the cores of the

(41) Mulder, C. A. M.; Damen, A. A. J. M. *J. Non-Cryst. Solids* **1987**, *93*, 169.
(42) Pouxviel, J. C.; Boilot, J. P.; Beloeil, J. C.; Lallemand, J. Y. *J. Non-Cryst. Solids* **1987**, *89*, 345.

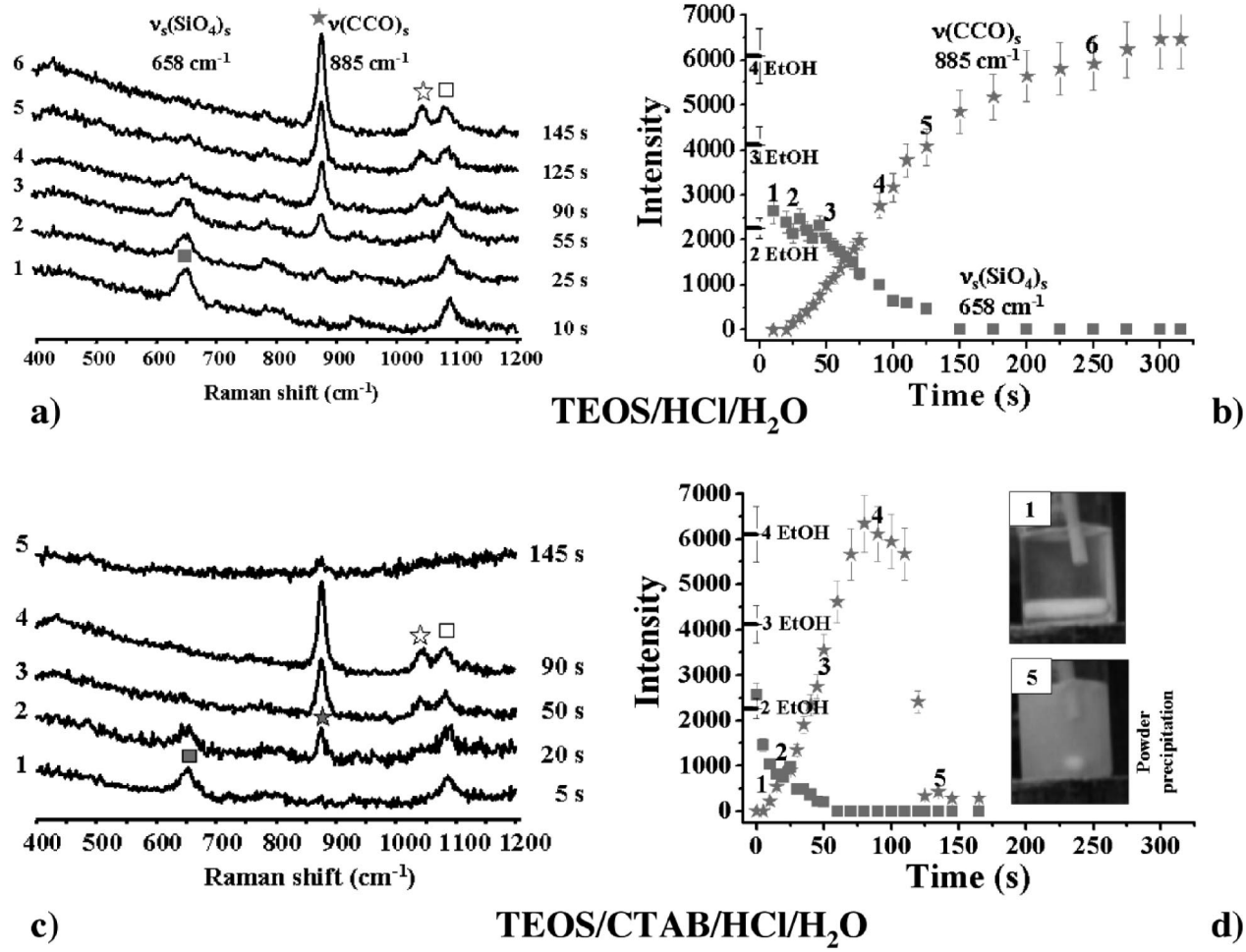

Figure 3. Time-resolved in situ Raman spectra of (a, b) TEOS/H_2O = 1/200 and (c, d) CTAB/TEOS/H_2O = 0.12/1/200 solutions corresponding to system B (C_{HCl} = 2.5 M). (a, c) Selected Raman spectra at different reaction times (t = 0 occurs at TEOS addition). (b, d) Time evolution of the integrated Raman intensities of the EtOH $\nu(CCO)_s$ and TEOS $\nu_s(SiO_4)$ bands at 885 at 658 cm^{-1}, respectively. Numbers from 1 to 6 in (b) and 1 to 5 in (d) correspond to selected spectra shown in (a) and (c), respectively. Labels on the vertical axes in (b) and (d) indicate theoretical Raman intensities corresponding to the hydrolytic release of the indicated numbers of EtOH molecules per TEOS. Pictures in (d) show the reaction beaker at t = 5 and 145 s.

oil droplets are difficult to hydrolyze compared to OH-substituted species which are located at the oil–water interface.

Bands for hydrolyzed monomers $Si(OEt)_{4-x}(OH)_x$ near 670 and 700 cm^{-1} have been reported;[41,43] these strongly overlap with the TEOS band, resulting in the detection of only one broad band shifted to higher wavenumbers. Such a shift was not observed in Figure 3a, suggesting the absence of hydrolyzed monomers having sufficient lifetimes to be detected. The formation of condensed species from OH-substituted monomeric species was thus anticipated. ^{29}Si NMR and Raman spectra recorded on solutions having a H_2O/TEOS molar ratio between 0.5 and 1.75 and mild acidic conditions (0.01–0.03 M HCl) have been compared,[36,41] and bands at 600, 576, 554, and 534 cm^{-1} have been assigned to $Si_2O(OEt)_6$ dimers, linear $Si_3O_2(OEt)_8$ trimers, and linear and branched $Si_4O_3(OEt)_{10}$ tetramers, respectively. The dimer and trimer bands have intensities comparable to that of the TEOS band at 658 cm^{-1}, while the tetramer bands are much weaker. Hence, the fact that we did not detect any band in the 500–600 cm^{-1} region indicated that few symmetric dimers and trimers were formed. Such species could have formed by condensation of monomeric $Si(OEt)_3(OH)$ species, since TEOS reacts predominantly by water-producing condensation reactions.[44] We thus assumed that under our experimental conditions, species that were located at the surface of the TEOS droplets experienced multiple hydrolysis steps and subsequent condensation reactions to form oligomeric polysiloxanes, which were released into the aqueous phase but could not be detected by Raman scattering, since this technique is sensitive to symmetric vibrations of short-chain siloxanes.

Figure 3c shows the in situ time-resolved Raman experiments in which CTAB as well as TEOS was present in the aqueous solution, which corresponded to system B (Table 2). First, it should be mentioned that contrary to the previous case, an emulsion having smaller and much more dispersed droplets was formed initially and then disappeared during the course of the reaction. The same TEOS and EtOH bands were detected, but the kinetics were different. The TEOS signal at 658 cm^{-1} rapidly decreased and vanished completely by t = 50 s. Simultaneously, the EtOH peak at 885 cm^{-1} rapidly grew in intensity until t = 90 s, at which time

(43) Barrie, J. D.; Aitchison, K. A. *Mater. Res. Soc. Symp. Proc.* **1992**, *271*, 225.

(44) Assink, R. A.; Kay, B. D. *Colloids Surf., A* **1993**, *74*, 1.

its intensity corresponded to $C_{EtOH}^{exp} = 0.95$ M, indicative of a TEOS hydrolysis degree of 90%. After $t = 90$ s, the intensity of the EtOH peak dropped to zero within a 20 s time span. As the images of the reaction beakers in Figure 3d show, powder precipitation occurred in the solution at that point; scattering due to silica particles was too important, and the Raman signal was lost. When CTAB was added to solution, the TEOS band disappeared when 2.5 EtOH molecules per TEOS were produced, corresponding to a total degree of TEOS hydrolysis of ~60%. This is lower than in the case of the CTAB-free system, for which the total degree of TEOS hydrolysis was ~70% when TEOS signal vanished. This tells us that the hydrolysis is more homogeneous in the presence of CTAB and further indicates the importance of solubilization and emulsion stabilization by CTAB. As already mentioned, in the absence of CTAB, a sizable fraction of the TEOS had not hydrolyzed at all at intermediate times, while many other TEOS molecules had gone through several hydrolysis steps within the same time period. Besides the effects of micellar solubilization and surfactant stabilization of emulsion droplets, it is possible to think of other factors that could enhance the hydrolysis of TEOS. For example, the chemical nature of the surfactant could also play an important role. To explore this, we also investigated (in a study that will be reported elsewhere) the effect of another type of surfactant, namely, the Pluronic block copolymer P123, whose chemical composition is totally different from that of CTAB. A similar large enhancement of the TEOS hydrolysis rate in the presence of the amphiphilic agent was found, suggesting that this behavior may be a general occurrence when micelle aggregates are introduced into an aqueous solution of TEOS and that it is related to the amphiphilic nature of the aggregates.

An overall hydrolysis rate constant k_H that corresponds to the average of those for various hydrolysis reactions (2) can be introduced:[45]

$$\equiv Si-OEt + H_2O \xrightarrow{k_H} \equiv Si-OH + EtOH \quad (2)$$

The rate law corresponding to 2 is

$$d[Si-OEt]/dt = -k_H[Si-OEt][H_2O] \quad (3)$$

In our system, one can assume that the concentration of water remains constant. Integration of eq 3 then gives

$$[Si-OEt]_t = [Si-OEt]_0 \exp(-k_H[H_2O]_0 t) \quad (4)$$

The time evolution of $[Si-OEt]_t$, the concentration of Si−OEt species, was obtained from the time evolution of the EtOH concentration in Figure 3b,d using the expression $[Si-OEt]_t = 4[TEOS]_0 - [EtOH]_t$. The resulting two curves were then approximated with a monoexponential function, according to eq 4, yielding k_H values of ~0.5 and ~1.0 M^{-1} h^{-1} for the systems without and with CTAB, respectively. This analysis using a "global" hydrolysis rate is of course oversimplified, but it confirmed literature reports of first-order kinetics for hydrolysis of TEOS in a water-rich medium.[21,42]

(45) Orcel, G.; Hench, L. *J. Non-Cryst. Solids* **1986**, *79*, 177.

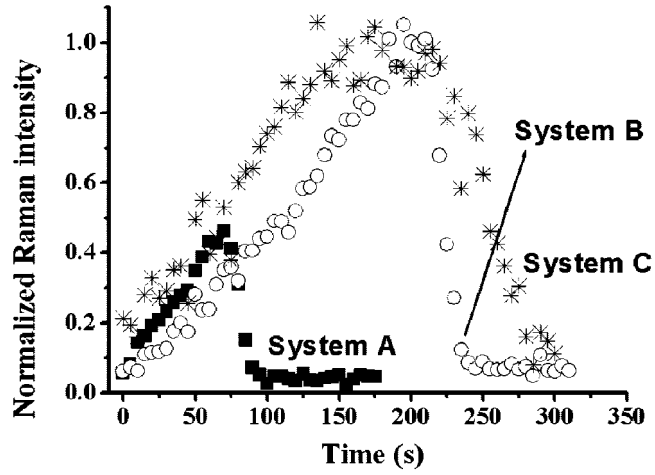

Figure 4. Comparison of intensities of the EtOH Raman peak at 885 cm^{-1} as a function of time for systems A (solid squares), B (open circles), and C (asterisks). The intensities have been normalized so that a value of 1 corresponds to complete TEOS hydrolysis (EtOH/Si = 4).

Since it is known that condensation reactions between silanol groups are highly favored in a water-rich medium,[44] an overall rate constant k_C for condensation reactions (5) can be defined in a similar way:

$$\equiv Si-OH + HO-Si\equiv \xrightarrow{k_C} \equiv Si-O-Si\equiv + H_2O \quad (5)$$

Under such conditions, the rate of EtOH release should depend only on the hydrolysis reactions.

For the purpose of comparison, an additional set of experiments with similar stirring conditions was performed on the three systems A, B, and C (Table 2). As shown in Figure 4, precipitation occurred at very different degrees of TEOS hydrolysis for systems A and B (50% and >90%, respectively). For system C, full hydrolysis was achieved before precipitation took place.

Interestingly, the rate at which EtOH was released was very similar for the three systems, confirming that dilution has little or no influence on hydrolysis reactions ([Si] = 0.08 M for system C and 0.43 M for system A). On the contrary, dilution plays a crucial role in the extent of TEOS condensation at the same acid concentration ($C_{HCl} = 3.9$ M): the lower the TEOS concentration in solution, the longer the time required for powder precipitation to occur. In addition, it may be observed that the silica-precursor and acid concentrations both play an important role in the reactivity of TEOS and oligomers derived from it, as shown by the fact that hydrolysis/condensation occurred faster in system A ($C_{HCl} = 3.9$ M) than in system B ($C_{HCl} = 2.5$ M). The effect of acidity on TEOS reactivity is a well-known result, as previously discussed in refs 21 and 41. However, the presence of CTAB in the initial acidic solution played a key role in the TEOS hydrolysis kinetics. The most plausible reason for the observed increase in TEOS hydrolysis in the presence of CTAB is the possibility of TEOS solubilization within micelles and/or kinetically stabilized emulsion droplets, which would increase the surface/volume ratio of the TEOS droplets and enhance TEOS−water contact, thus leading to a higher TEOS hydrolysis rate. Hydrodynamic

effects related to the stirring speed have previously been shown to have a pronounced influence on the hydrolysis kinetics of TEOS under alkaline conditions.[46] The importance of solubilization effects is highlighted by the fact that the observed hydrolysis rate was proportional to the CTAB concentration in the sol and the solubilization power of CTAB calculated per molecule should increase when the CTAB concentration is higher than the critical micelle concentration. The high ionic strength of the sol, which is due to the high concentrations of HCl, should further enhance the solubilization capacity of CTAB, as the repulsive charges between the surfactant head groups in a surfactant aggregate would be effectively screened, stabilizing the surfactant aggregate of lower curvature. The influence of CTAB on the hydrolysis kinetics should then be greatest at the early stages of the reaction, as TEOS is a very hydrophobic molecule and will be solubilized inside the interior of the micelles. As the hydrolysis proceeds, the water solubility of the partially hydrolyzed TEOS molecules increases; thus, the preference for solubilization within surfactant aggregates is reduced, and further hydrolysis can occur outside the micelle aggregates.

In Situ SAXS/XRD Experiments. Time-resolved in situ SAXS/XRD experiments were used in order to follow the mesophase evolution. Time-resolved XRD patterns for systems A−C and surface plots of the same measurements are shown in Figure 5. Because the TEOS hydrolysis kinetics was found to be strongly dependent on the stirring rate, the phase-separation kinetics was also followed by a video camera, and the times at which the first signs of a Bragg reflection (10) appeared in the diffractograms corresponded to the times at which the sols turned milky. This allowed us to establish a direct link between the Raman measurements and the XRD measurements, although the stirring rates may have been slightly different in the two sets of experiments. The time at which the (10) reflection of the 2D hexagonal mesophase appeared in the different cases was strongly system-dependent and followed the order of the TEOS/CTAB concentrations in the sols. For the most concentrated system, A, the (10) reflection was seen after a reaction time of 50 s, which corresponded to a total degree of TEOS hydrolysis of 50% and was in good agreement with the time at which the solutions became turbid in the Raman experiments. For system B, the (10) reflection was visible 80 s into the reaction, which corresponded to 90% hydrolysis of TEOS. For the most dilute system, C, the first sign of a (10) reflection was seen after a reaction time of 250 s, while complete hydrolysis of the TEOS had been reached earlier, in less than 200 s. Taking into account the concentration differences in the different systems (the ratios of the TEOS concentrations in the starting sols were $C_{Si}^{A}/C_{Si}^{B}/C_{Si}^{C} \approx 5.4/3.5/1$), one can see that the total extent of hydrolysis at which some degree of order was observed in the diffractograms was similar for systems A and B, while the kinetics of formation of an ordered silicate/surfactant phase occurred at a lower total concentration of hydrolyzed TEOS in the sol for system C. For system A, the (11) and (20) reflections appeared at virtually the same time, while for systems B and C, the (20) reflection appeared before the (11) reflection. This suggests that the silica-wall thickness was larger for system B than for system A, as the Fourier phasing (results not shown) was found to be $- + +$ for the (10), (11), and (20) reflections, which is similar to that observed for MCM-41.[46] While the higher-order reflections appeared just after the (10) reflection in system A, there was a time difference of 50 s for system B and 150 s for system C. In addition to the (10), (11), and (20) reflections characteristic of a 2D hexagonal mesophase, a broad reflection of low intensity at lower angles ($q \approx 1.1$ nm^{-1}) was observed (Figure 5c) after a reaction time of 800 s. This reflection, whose origin is not known, could indicate the presence of another coexisting phase of low concentration and mesoscopic order.

The position of the main (10) reflection for each system is plotted as a function of time in Figure 6. The positions of the (10) reflection at the time of its first appearance were 4.22, 4.29, and 4.31 nm for systems A, B, and C, respectively. Furthermore, in all of the systems, the *d*-spacing decreased with reaction time at a rate that was proportional to the TEOS/CTAB concentration. Two distinctively different stages in the decrease in the *d*-spacing with time were observed, the kinetics of which were also strongly dependent on the sol composition. For systems A and B, in all cases a moderately fast decrease in the *d*-spacing was observed until a reaction time of 500 s, after which a second stage of slower but almost linear decrease occurred. For system C, on the other hand, the position of the (10) reflection remained virtually constant during the time of observation. The time at which the second stage was reached depended strongly on concentration: the second stage was observed to begin at 500 s for system A and at 1400 s for systems B and C, although for system C the decrease was not as evident as for system B. (The evolution of the position of the higher-order reflections with time in Figure 5 should also be noted.) At the intermediate plateau, the corresponding distances (calculated directly as $d = 1/s$) were 4.12 and 4.24 nm for systems A and B, respectively, indicating only a marginal decrease in the repeat distance during the first phase. We note that this small decrease in the unit-cell dimensions could not be connected to the decrease in micelle diameters due to release of hydrolyzing TEOS from the interior of the micelles, because the decrease in the unit-cell dimensions occurred at times well past that needed for complete hydrolysis of TEOS in system B. At a reaction time of 2000 s (i.e., well within the second stage of the process), the corresponding values were 4.03 and 4.17 nm for systems A and B, respectively, which translate to unit-cell sizes of 4.65 and 4.81 nm, respectively. Thus, the repeat distances in the silicate/surfactant phase at all times followed the order of TEOS/CTAB concentration in the initial sol; the higher the initial TEOS/CTAB concentration, the smaller the repeat distance. This behavior was also observed for the as-synthesized, dried materials isolated after a complete synthesis ($t = 180$ min): the *d*-spacings were 3.71, 3.82, and 3.87 nm for materials synthesized using systems A, B, and C, respectively (results not shown).

The integrated intensities of the (10) reflection are plotted as a function of time in Figure 7. For all of the systems, an exponential increase in the integrated intensity was observed during the time window corresponding to the first stage of the

(46) Beurroies, I.; Ågren, P.; Bulchel, G.; Rosenholm, J. B.; Amenitsch, H.; Denoyel, R.; Lindén, M. *J. Phys. Chem. B* **2006**, *110*, 16254.

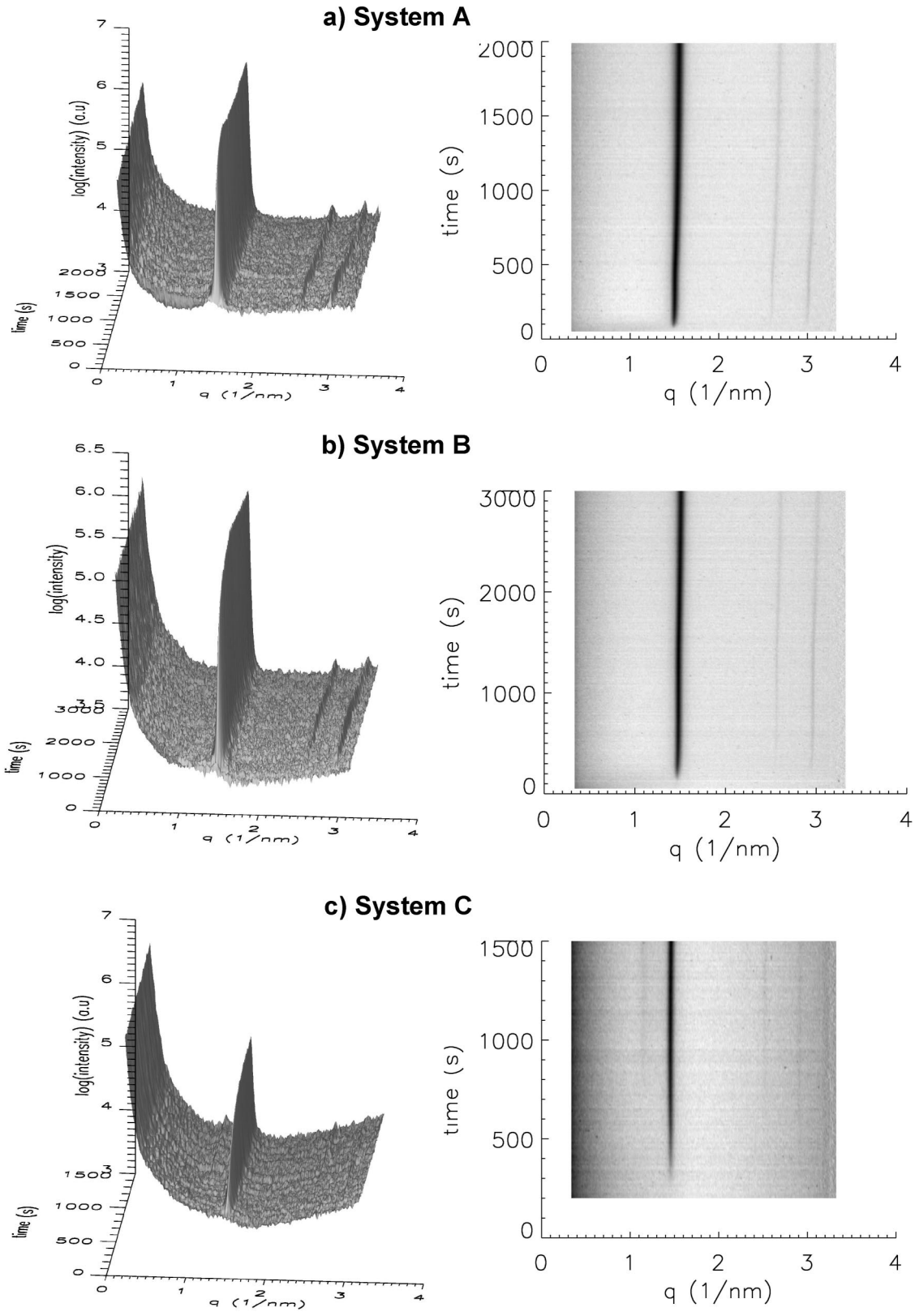

Figure 5. Left column: Time-resolved XRD patterns showing the formation of SBA-3 for systems A−C. See text for details. A data sampling time of 10 s/frame was used. Data were not background-corrected. Right column: Surface plots corresponding to the time-resolved XRD patterns for systems A−C. Data were background-corrected.

decrease in the *d*-spacing shown in Figure 6. The rates at which the intensity increased during this stage followed the order system C < system B < system A (i.e., the order of increasing TEOS/CTAB concentrations in the starting sols). For systems B and C, the intensity then reached a plateau, while for system A, the intensity increased almost linearly at reaction times corresponding to the second stage of the decrease in the *d*-spacing shown in Figure 6. Furthermore, it is interesting to note that the ratios of the integrated intensities after the first stage (i.e., after reaction times of 500, 1000, and 1500 s for

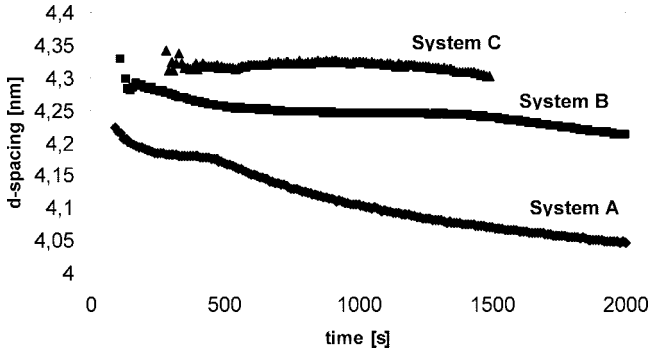

Figure 6. Time evolution of the positions of the (10) reflection of the 2D hexagonal SBA-3 phase for systems A (diamonds), B (squares), and C (triangles).

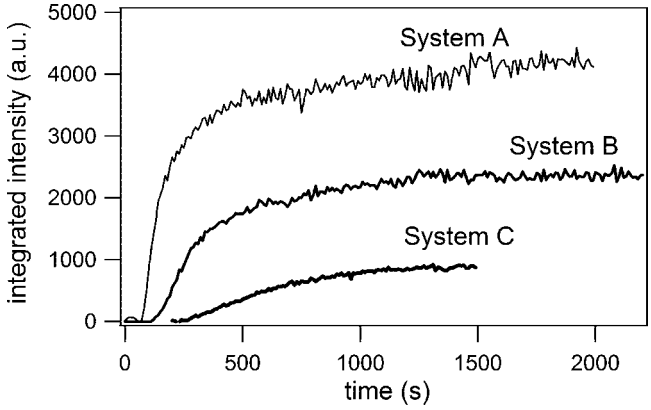

Figure 7. Time evolution of the integrated intensities of the (10) reflection of the 2D hexagonal SBA-3 phase for systems A−C.

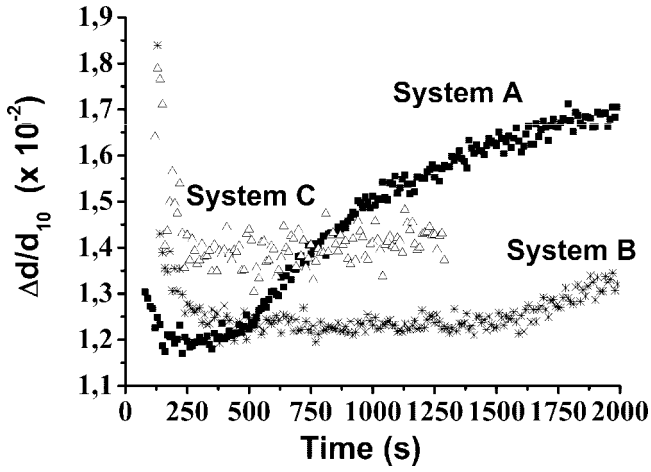

Figure 8. Time evolution of the normalized full widths at half-maximum $\Delta d/d_{10}$ of the (10) reflection of the 2D hexagonal SBA-3 phase for systems A (solid squares), B (asterisks), and C (open triangles).

systems A, B, and C, respectively) virtually exactly followed the corresponding ratios of the initial CTAB/TEOS concentrations in the different sols. This suggests that the amount of phase-separated silicate/surfactant (normalized against the initial CTAB/TEOS concentration) was virtually the same in all cases.

Finally, the time evolution of the full width at half-maximum (fwhm) of each (10) reflection is shown in Figure 8. Each fwhm value was normalized against the position of the (10) reflection in order to make direct comparisons of the different fwhm values possible. For all of the systems, there was a pronounced initial decrease in the fwhm during the first 100–150 s after the formation of the 2D hexagonal phase, and the absolute fwhm values during this phase were inversely proportional to the CTAB/TEOS concentrations in the sols (i.e., the absolute fwhm values followed the order system A < system B < system C). This initial phase was followed by an intermediate phase in which the fwhm values remained virtually constant. The fwhm values for systems A and B started to increase again after reaction times of 500 and 1500 s, respectively. This third phase of increasing fwhm values occurred at reaction times corresponding to the second reaction stage observed in the plots of *d*-spacing versus time (Figure 6). For system C, no such increase in the fwhm maximum value was observed during the time of observation.

General Mechanistic Discussion. Overall, our data are in full agreement with the common understanding that the formation of silicate/CTAB mesophases in dilute sols using alkoxides as the silica precursor involves the following steps: (1) hydrolysis of the silica precursor followed by condensation, leading to the formation of oligomeric siliceous species (here the hydrolysis kinetics of the silicon alkoxide is greatly enhanced in the presence of the surfactant as a result of micellar solubilization and surfactant stabilization of emulsion droplets); (2) phase separation into one phase rich in silicate and surfactant and another phase rich in solvent; and (3) nucleation and growth of a surfactant/silica mesophase in this concentrated phase. The different reaction steps can partially overlap. However, the fact that we carried out the measurements under different degrees of dilution and also measured the extent of TEOS hydrolysis as a function of time allows us to draw some additional conclusions about the chemical events leading to the formation of the 2D hexagonal phase and the influence of their relative rates.

First of all, from our Raman scattering data it is clear that the time at which phase separation occurred (indicated by the appearance of turbidity in solution) was related not to the relative extent of TEOS hydrolysis but instead to the absolute concentration of hydrolyzed species (system A > system B > system C), as indicated by the observed kinetics. However, this is not the whole truth, as phase separation can occur after complete hydrolysis of TEOS, whose absolute concentration was lower in system C than in systems A and B. Our results thus indicate that the condensation kinetics was also a crucial parameter in the formation of SBA-3 and that a certain level of silicate condensation had to be reached before phase separation occurred.

As a consequence of the previously described behavior and after analysis of the SAXS experiments, it is plausible that the first step observed in the plots of *d*-spacing versus time (Figure 6) was connected to a correlation distance in the phase-separated silicate/surfactant phase and that the nucleation and growth of the 2D hexagonal phase was very fast within this phase. Unfortunately, the low micellar scattering intensity did not allow us to determine the shape of the micelles in the phase-separated silicate-surfactant phase. However, on the basis of the short correlation distance observed, which indicates that the silicate/surfactant phase was relatively concentrated, one can assume that cylindrical micelles were present. Once ordering occurs, the single (10) reflection that was observed for different times in all of the systems prior to the appearance of the higher-order

reflections is normally observed for wormhole-like materials, which are formed from entangled micelles. However, we note that a single reflection with a repeating distance larger than that normally found for 2D hexagonally ordered MCM-41-type materials has also recently been observed for mesoscopic silicate/CTAC nanoparticles synthesized under alkaline conditions.[47] On the basis of detailed analysis of the time-dependent fwhm values of the reflections, a recent study on MCM-41[46] suggested that local differences in the degree of silicate condensation were present within growing domains having hexagonal order. It was also suggested, on the basis of earlier TEM studies,[48] that the cylinders inside the domains were more tightly packed than those on the rim of the particle facing the solution during the stages where the silicate condensation reactions were still ongoing. The formation of larger aggregates that dry/condense faster in more concentrated sols would work in the direction of tighter micelle packing, at least during the early stages of the formation process. These considerations could explain the differences in the repeating distances observed for the different systems as well as the reason why system C did not reach the second stage of the process, in which the 2D hexagonal phase nucleated and grew: despite the fact that the local concentrations of silicate and surfactant were high, the particle size may still have been very small during the initial stages of the process, leading to slower particle growth by aggregation.

Further support for the idea that nucleation and growth in system C was slower than in systems A and B can be actually found in a recent study involving MCM-41-type materials,[47] where domain growth by particle fusion was observed under alkaline conditions. This could be another process that is strongly bound to particle concentration. This view is supported in our work by the evolution of the unit-cell dimensions obtained for systems A−C (Figure 6). However, the time evolution of the normalized fwhm values of the (10) reflection was very different than that observed during the formation of MCM-41 at a pH of 10.8.[46] In that work, the normalized fwhm of the (10) reflection decreased very soon after the 2D hexagonal phase appeared and remained virtually constant during the observation time. A similar evolution of the fwhm of the main reflection was also observed for SBA-15 synthesized under acidic conditions using nonionic triblock copolymers as the structure-directing agent.[9] However, the observation time in the present study is longer than that in the MCM-41 study, and the initial evolution of the normalized fwhm values of the (10) reflection (i.e., a fast initial decrease followed by a period where the fwhm remained constant) was similar in all three cases. The subsequent increase in the normalized fwhm values of the (10) reflection during the later stage of the process, which was accompanied by a decrease in the mean *d*-spacing, can then be connected to an increase in dispersion due to coexistence of portions of the sample which had undergone local intermicellar condensation with portions where the amount of intermicellar condensation was still small. The most homogeneous nucleation and growth, but also the lowest growth rate, was observed for the most dilute system, C, which completely hydrolyzed before phase separation into the silicate/surfactant-rich phase occurred. Greater sol dilution should slow the particle–particle aggregation process, which is another important step in mesophase formation. Now, the time evolution of the fwhm values of systems A and B also suggests that the particle–particle aggregation kinetics played an important role, as previously observed for MCM-41:[46,47] particle–particle aggregation can cause the particles to dry faster as a result of decreased particle–water contact area.[48] This process should be accompanied by faster condensation in the hexagonally ordered phase, as indicated by both the lower *d*-spacing observed at higher CTAB/TEOS concentrations and the fact that increases in the ratio of intensities of the (11) and (20) reflections were more pronounced for the slower-reacting systems B and C as well as by the initial absence of the (11) reflection. Differences in the relative rates of domain growth in the 2D hexagonally ordered portions and of particle–particle aggregation may also have contributed to the observed differences in the fwhm values between the systems. In fact, particle–particle aggregation that is fast compared with domain growth may induce disorder if oriented attachment effects are not prevalent.

A second point to be discussed is the evolution of the (11)/(20) intensity ratio, which was compatible with an increase in the silicate layer thickness relative to the radius of the micelles, as discussed in ref 46 after a fine analysis of phasing-coefficient signs in the Fourier transform of the diffraction-peak intensities. In our work, the absence of the (11) reflection during the initial stages for systems B and C suggests that these systems were at the borderline between Fourier phases $-\,+\,+$, which was observed for MCM-41,[46] and $-\,-\,+$, which was observed for SBA-15.[9] This is another indication of thicker silicate walls in systems B and C compared with system A, resulting from lower TEOS/CTAB concentrations.

Finally, we note that although the phase-separation kinetics in the studied systems was compatible with that of MCM-41 synthesized using ammonia as the catalyst, the growth kinetics of the mesophase was slower. This can be ascribed both to a lower overall silicate condensation rate for the SBA-3 system under the conditions employed here compared with that for MCM-41 synthesized in the presence of ammonia and to slower overall-ordering kinetics. In this respect, the absence of strong electrostatic interactions between the positively charged structure-directing agent and the silicate species under acidic conditions, where the silicate species are nearly neutral or have slightly positive charge, also may have influenced the silicate condensation kinetics in the mesophase. Under alkaline conditions, where the silicate species have a negative charge, the formation of cylindrical micelles should be faster than under acidic conditions, since surfactant charge neutralization favors the transition from spherical to cylindrical micelles,[49] which should increase the rate of ordering in the mesophase.

CM702128U

(47) Möller, K.; Kobler, J.; Bein, T. *Adv. Funct. Mater.* **2007**, *17*, 605.
(48) Sadasivan, S.; Fowler, C. E.; Khushalani, D.; Mann, S. *Angew. Chem., Int. Ed.* **2002**, *41*, 2151.
(49) Friman, R.; Backlund, S.; Hassan, O.; Alfredsson, V.; Lindén, M. *Colloids Surf., A* **2006**, *291*, 148.